Salt intrusion

due to tidal influences in estuarine environments

by

L.M.J. van Tol

to obtain the degree of Bachelor of Science in Applied Mathematics
and in Applied Physics at the Delft University of Technology,
to be defended publicly on December 12, 2024.

Student number: 5144639
Project duration: July, 2024 – December, 2024
Thesis committee: Dr.ir. Y.M. (Yoeri) Dijkstra, (supervisor)
Prof.dr.ir. C.R. (Chris) Kleijn, (supervisor)
Dr. B (Bijoy) Bera,
Prof.dr.ir. M.B. (Martin) van Gijzen

TU Delft

Abstract

This thesis focuses on the influence of tides on flow behaviour and salt intrusion in a semi-infinite channel ending at the sea, with a specific focus on the effects of adding a side channel. Tide causes variations in the flow behaviour, which in turn affects salt concentrations in the channel. Adding a side channel has an impact on the flow pattern, mainly because of reflections of the tidal wave, leading to changes in the salt intrusion. The effect investigated is the influence of varying the distance from the sea to the junction, and the length of the side channel. A 1-dimensional exploratory model based on the shallow water equations for the flow behaviour is developed, analysing only the bidaily M2 tide caused by the gravitational pull of the moon. The flow pattern is solved analytically, while the salt balance is solved analytically in time but numerically in space. The salt balance contains an advection term and an effective dispersion term. The effect of adding a branching channel is compared to the same situation without a branching channel. It is found that the addition of a side channel affects the salt intrusion in the order of 1 km compared to a single channel. Moreover, both positive and negative changes occur in the shift of the intrusion length. The results of this study can be used to understand and explain the behaviour in more complex geometries.

Nomenclature

System properties

Symbol	Definition	Unit
w	width of the channel	m
h	dept of the channel	m
τ	bottom stress	$\mathrm{kg\,m\,s^{-2}}$
ρ	water density	$\mathrm{kg\,m^{-3}}$
c_d	drag coefficient	$-$
k	effective dispersion prefactor	$-$
ω	angular frequency of the tide	$\mathrm{rad\,s^{-1}}$
A	amplitude of the tide	m
ϕ_0	tidally averaged discharge	$\mathrm{m^3\,s^{-1}}$
s_*	salt concentration in the sea	$\mathrm{kg\,m^{-3}}$
U	typical velocity in the channel	$\mathrm{m\,s^{-1}}$
L_1	distance between the sea and the split	m
L_2	length of the side channel	m
L_3	length of the numerical domain for the main channel	m

Derived properties

Symbol	Definition	Unit
r	friction factor	$\mathrm{s^{-1}}$
c	tidal wave velocity (without friction)	$\mathrm{m\,s^{-1}}$
c'	tidal wave velocity (including friction)	$\mathrm{m\,s^{-1}}$
$s(x,t)$	salt concentration	$\mathrm{kg\,m^{-3}}$
$\hat{s}(x,t)$	scaled salt concentration	-
$\eta(x,t)$	water height deviation	m
$\phi(x,t)$	water flow	$\mathrm{m^3\,s^{-1}}$
$v(x,t)$	water velocity ϕ/wh	$\mathrm{m\,s^{-1}}$
$\mathbb{D}$	effective dispersion coefficient	$\mathrm{m^2\,s^{-1}}$
L	characteristic intrusion length	m

Other

Symbol	Definition	Unit
x	distance	m
$\hat{x}$	scaled distance	-
t	time	s
g	gravitational acceleration	$\mathrm{m\,s^{-2}}$

Contents

1 Introduction

The Netherlands has a long and impressive history with the sea. But living in harmony with the sea requires a deep understanding of its effects. One of the effects, of course, is the sea's ebb and flood tide behaviour. Tide is the periodic rise and fall of the water level. This is influenced by many different factors, but one of the biggest influences comes from the gravitational pull of the moon. This contribution is called the M2 tide, since it is caused by the Moon and occurs twice a day. The M2 tide has a period of $T = 12.42\mathrm{h}$.

A river flowing into the sea, which is an estuarine environment, is influenced by this. If the water level of the sea is higher than that of the river, water can start flowing from the sea into the river. This is when salt from the sea is carried into the freshwater river. This process is called salt intrusion, and it can have an effect on the ecology of the river[7]. The mixing of salt and freshwater creates brackish water, and this is a biotope in which some plants and animals thrive. It can furthermore have an effect on the irrigation used for agriculture [11] and it can have an effect on drinking water extraction, because salt is hard to filter[5]. There is even a global campaign on salinization by the united nations which has as an objective to raise awareness among researchers, as well as other groups e.g. policy makers[9]. It is therefore of importance to understand the underlying mechanism of the salt transport.

If a branching channel or a port is added to the river and a junction is formed, the flow behaviour is altered and thus the salt intrusion as well. Furthermore, if the river already has a branching channel and a weir is placed in it, the flow behaviour is also altered. It is therefore of importance to understand what effect these interventions can have on the salinization in the river. To understand the physics behind the salinization, a model is needed for the process behind salt intrusion. There are three common ways to model salt intrusion. These are a perfectly mixed system in the vertical direction, a two-layer system or a partially mixed system. Of these three, the perfectly mixed model is the simplest.

Several articles provide more insight into the dynamics inside estuaries and the way in which salt in estuaries can be modelled. In Ippen[4] it is described how tidal influences in estuaries can be modelled for estuaries with constant cross-sections and for channels with gradually varying sections. In Schijf[12] a two-layer system is developed for the salt concentration. This is a model in which the salt and freshwater layers are sharply separated. In MacGready[6] a model for the tidally-averaged salinity of a channel system with varying cross-sections is developed and solved numerically. This model does not assume the salt to be perfectly mixed vertically. In Siles-Ajamil[13], an exploratory model incorporating salt dynamics is used to review the impact of various interventions on salt intrusion and tidal amplitudes in a specific estuary, which is modelled as a network of interconnected channels. In Alebregtse[1] the effects of a branching channel (with friction) on the flow behaviour is analysed for a system consisting of two closed channels and an open boundary at sea. It is shown that phase shifts and resonance can occur depending on the distance between the sea and the junction and the length of the branching channel. What has not been researched yet is the effect that this interference pattern can have on the salt intrusion. This is relevant when human interventions, such as adding a side channel or placing a weir in a side channel, are considered.

This bachelor thesis makes a step in improving the understanding of the mechanism of salt intrusion in estuarine environments with branching channels by utilising a simple exploratory model. This model is based on the 1-dimensional shallow water equations for the flow behaviour and a 1-

dimensional advection-dispersion equation for the salt concentration. A sketch of the junction is provided in figure 1.1. Its aim is not to provide a perfect description of the real-world conditions, but to be a tool to be used in the explanation of more complex geometries. The key question addressed here is: *What is the effect of varying the distance between the sea and the junction and the length of the branching channel on the salt intrusion?*

To answer this question, two situations will be discussed. The first situation is a semi-infinite constant width and constant depth channel which is connected to the sea at one end. This will mainly be used as a reference for the second situation. The second situation that is analysed is the addition of a finite (closed at one end) constant width and constant depth channel to the semi-infinite one. It has already been shown that in this situation resonance can occur [1], and the effects of the interference of the tidal waves on the salt intrusion is analysed.

We will start the examination by first creating a 1-dimensional model for the tidal flow in both geometries and solving this analytically. Subsequently we will extend this model to describe the salt transport. This is done in chapter 2. Next, the results are shown and discussed, this is done in chapter 3. Finally, in chapter 4, we will summarize the main findings and suggest potential directions for further research.

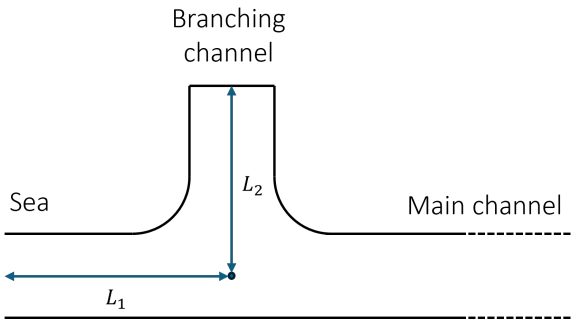

Figure 1.1: Sketch of a branching channel added to a main channel and the distances that can be varied. The horizontal arrow is the distance between the sea and the split, the vertical arrow is the length of the branching channel.

2

Model

The goal is to describe the influence of a branching channel on the salt concentration. However before we can describe the salt concentration, we first need to know the flow behaviour. Therefore we will split the problem into two parts. First we will develop a model for the flow behaviour. This is done in section 2.2. It is first done for a semi-infinite channel and subsequently for a branched channel. Once this is completed we can construct a salt balance which uses the flow behaviour. This is done in section 2.3. This is again done first for a semi-infinite channel and finally for a branched channel. We will end the chapter with a section describing a method for the analysis of the results.

2.1. Problem description

We will now continue with the problem description of the single channel, this will later in the chapter be expanded to a branched channel system. First, we assume the channel has a constant width w and a constant depth h. The depth is measured as the average of the water height over a full period of the tidal wave, and thus not dependent on time. The change in water height, compared to the average, will be denoted by $\eta(x,t)$. At one end it is connected to the sea (at $x = 0$), and at the other end it stretches to infinity ($x \to \infty$). Furthermore, the channel has a regular discharge which is not influenced by tide. We will call this discharge ϕ_0. We furthermore assume the water to be of the same density everywhere. Moreover we assume the tide and the salt concentration at sea s_* not to be influenced by the channel dynamics. The component of the tide that we are interested in is the bidaily M2 tide. This is the component that is caused by the gravitational pull of the moon. It can be described as a sine with period 12.42h. This means that is has an angular frequency of $\omega = \frac{2\pi}{T} \approx 1.405 \cdot 10^{-4}\text{s}^{-1}$. The problem we are facing is sketched in figure 2.1.

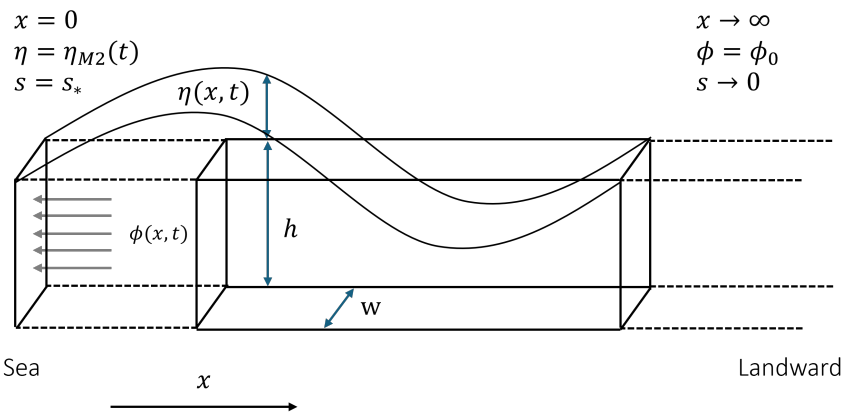

Figure 2.1: The single channel geometry.

2.2. Water height and flow rate

In this section we start by developing a model for the water height and the flow rate. First the shallow water equations are introduced, and subsequently they are solved for a single semi-infinite channel and a main channel with a connected side channel.

2.2.1. Wave equation

Our starting point is the derivation of the governing wave equation. This can be derived by using two equations. The first equation is the conservation of mass (2.1). This equation denotes that a spatial difference in flow (ϕ) (r.h.s.) causes the water level (η) to rise (l.h.s.). This rise in water level depends on the width (w), since if the channel is narrower the water level rises quicker than if the channel was very wide. This can be written as

$$w\frac{\partial \eta}{\partial t} = -\frac{\partial \phi}{\partial x}. \tag{2.1}$$

The second equation is the conservation of momentum over a control volume (2.2). The terms from left to right are; the change in momentum over time, the transport of momentum, the gravitational force and the friction of the riverbed. This leads to,

$$\frac{1}{wh}\frac{\partial \phi}{\partial t} + \frac{\phi}{(wh)^2}\frac{\partial \phi}{\partial x} + g\frac{\partial \eta}{\partial x} + \frac{\tau}{\rho h} = 0. \tag{2.2}$$

There are some simplification we can do to make the equations easier to solve. The bottom stress τ in the friction term in equation (2.2) depends quadratically on the velocity of the water and is therefore not linear. This makes the equation more difficult to solve compared to a linear term. We can linearize the friction term as $\frac{\tau}{\rho h} = \frac{r}{wh}\phi$ with friction factor $r = \frac{c_d}{h}\frac{8U}{3\pi}$ using a Fourier expansion in which U is a typical velocity in the channel and c_d is a bottom friction coefficient[10]. Furthermore, the convection term $\frac{\phi}{(wh)^2}\frac{\partial \phi}{\partial x}$ is usually small for tidal flow[2] and hence is neglected. These two equations can be combined (see appendix A.1) to form the following wave equation:

$$\frac{\partial^2 \eta}{\partial t^2} + r\frac{\partial \eta}{\partial t} = gh\frac{\partial^2 \eta}{\partial x^2} \tag{2.3}$$

Alternatively, this can be derived using the shallow-water equations. These equations are simplifications of the Navier-Stokes equations by depth- and width-integrating them and assuming the vertical velocity is small compared to the horizontal velocity. For equation (2.3) it is natural to define $c = \sqrt{gh}$, as the wave velocity in the absence of friction. The friction term and the angular frequency of the tide will affect the final wave velocity. Note that the two equations (2.1 & 2.2) also could have been combined to form exactly the same equation in terms of ϕ.

$$\frac{\partial^2 \phi}{\partial t^2} + r\frac{\partial \phi}{\partial t} = gh\frac{\partial^2 \phi}{\partial x^2} \tag{2.4}$$

2.2.2. Semi-infinite channel

We will now proceed with solving equation (2.3) for the single channel. The geometry of the problem is sketched in figure 2.1. We are interested in the dynamic equilibrium solution. This is because the initial conditions will dissipate due to the friction and is therefore not of interest. Therefore we do not need the initial conditions. We are dealing with a second-order linear partial differential equation, hence we need two boundary conditions. We describe the boundary condition at the sea side ($x = 0$) as a wave with a fixed amplitude (A) independent of the channel. The wave has a certain period (for the M2 tide this is typically 12 hours and 25 minutes) which is contained in the angular frequency ($\omega = \frac{2\pi}{T}$) and a certain phase difference (θ). This leads to

$$\eta(0,t) = A\sin(\omega t + \theta). \tag{2.5}$$

At the other end (landward), we require that the tidal wave is bounded as $x \to \infty$. This means we have $\eta < \pm B$ as $x \to \infty$.

Now we have the problem clear, we can proceed by applying a Fourier transform in the time variable. This changes the partial differential equation into an ordinary differential equation in the x variable (2.6) which is easier to solve.

$$\frac{\partial^2 \mathcal{F}\{\eta\}}{\partial x^2} = -\frac{\xi^2 + r\xi i}{c^2}\mathcal{F}\{\eta\} \tag{2.6}$$

We define $\lambda^2(\xi) = -\frac{\xi^2 + r\xi i}{c^2}$. Note that λ is imaginary, its real part satisfies $\mathbb{R}\text{e}\{\lambda\} > 0$ (see A.2), and we have $\lambda(-\xi) = \overline{\lambda(\xi)}$. With the overline denoting the complex conjugate. The general solution for (2.6) is:

$$\mathcal{F}\{\eta\} = c_1(\xi)e^{-\lambda x} + c_2(\xi)e^{\lambda x} \tag{2.7}$$

First we will use the landward boundary condition. The tidal wave is bounded as $x \to \infty$. This means that $\mathcal{F}\{\eta\} < \pm B'$ as $x \to \infty$. Since $\mathbb{R}\text{e}\{\lambda\} > 0$ and $e^{\lambda x} = e^{\mathbb{R}\text{e}\{\lambda\}x}e^{\mathbb{I}\text{m}\{\lambda\}xi}$ this can only happen if $c_2 = 0$.

Secondly we will use the seaward boundary condition. We apply a Fourier transform to equation (2.5), and this leads to the following expression for c_1:

$$c_1(\xi) = \frac{Ai}{2}\left(e^{-i\theta}\delta(\xi - \omega) - e^{i\theta}\delta(\xi + \omega)\right) \tag{2.8}$$

If we now apply the inverse transform to (2.7) we get our final solution for the semi-infinite channel.

$$\eta(x,t) = Ae^{-\mathbb{R}\text{e}\{\lambda(\omega)\}x}\sin\left(\mathbb{I}\text{m}\{\lambda(\omega)\}x + \omega t + \theta\right) \tag{2.9}$$

In the solution we see a wave decaying exponentially as x becomes larger, with the wave oscillating in space and time. A solution for ϕ can be constructed using equation (2.1 or 2.2). It will be a superposition of the tidally averaged part (ϕ_0) and the tidally influenced part.

2.2.3. Branched channels

Now we turn our attention to a side channel connected to a main channel. The geometry of this situation is sketched in figure 2.2. The channel connecting the sea with the junction will be called the sea channel and will have subscript 1, the side channel has subscript 2 and the last channel will be called the main channel with corresponding subscript 3. We can view this problem as three separate branches with coupled boundary conditions. Hence, the governing equation is still wave equation (2.3). However, since it will make the analysis easier, we will complexify the wave equation and take the real part of the complex solution. The complex wave height and the complex flow will be denoted by a bold symbol, respectively $\boldsymbol{\eta}$ and $\boldsymbol{\phi}$.

As previously mentioned, we are interested in the dynamic equilibrium. Therefore we do not need initial conditions. For each branch we need two boundary conditions. We will start with the boundary conditions at the junction. At the junction we require the water level to be continuous, this leads to $\eta_1(0,t) = \eta_2(0,t)$ and $\eta_2(0,t) = \eta_3(0,t)$. Additionally we need to have that the flow into the junction equals the flow out of the junction (conservation of mass). This means we demand that $\phi_1 + \phi_2 + \phi_3 = 0$.

We will now continue with the boundary conditions for the other ends. For the boundary of the sea channel we prescribe the boundary as a complex exponential with angular frequency ω and complex amplitude A,

$$\boldsymbol{\eta}_1(L_1,t) = Ae^{i\omega t}. \tag{2.10}$$

For the side channel we require that $\phi_2(L_2,t) = \phi_{2,0}$, this means that we require the flow at the boundary to equal a constant flow $\phi_{2,0}$ not depending on time (for example due to a weir). If we set this constant $\phi_{2,0} = 0$ this would correspond to a hard wall. Conversely, setting it to a different value can be interpreted as a weir that regulates a constant discharge into the channel. Last but not least, for the main channel we require that η is bounded ($\eta_3(x,t) < \pm B$) as $x \to \infty$. Alternatively we can also prescribe a similar boundary condition as the side channel, if we want to represent a weir.

We can now continue with solving the problem. From our analysis of the semi-infinite channel the following structure for solutions with periodic forcing at the boundary is suggested:

$$\boldsymbol{\eta} = Z(x)e^{i\omega t} \tag{2.11}$$

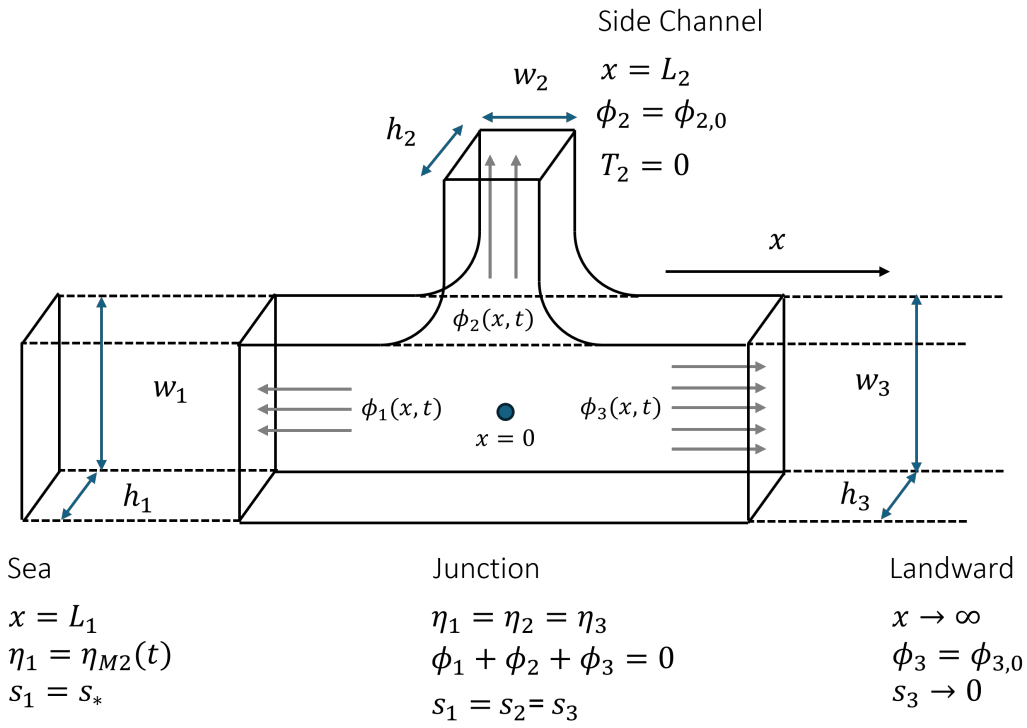

Figure 2.2: The geometry of the branched channel situation.

If we substitute this back into the (complex) wave equation we see that:

$$Z(x) = \alpha(\omega)e^{-\lambda(\omega)x} + \beta(\omega)e^{\lambda(\omega)x} \tag{2.12}$$

with λ defined slightly differently (compared to the semi-infinity channel) as $\lambda^2 = \frac{-\omega^2 + r\omega i}{c^2}$. To determine the coefficients α and β we use the 6 boundary conditions.

We can rewrite all boundary conditions as a system of six linear equations for the coefficients $\alpha_1, ..., \beta_3$. From the top to bottom row these represent (1) & (2): continuous water level, (3) conservation of flow, (4) bounded at infinity, (5) constant flow at the boundary, (6) tide behaviour at sea side. This is explained in more detail in the appendix.

$$\begin{bmatrix} 1 & 1 & -1 & -1 & 0 & 0 \\ 0 & 0 & 1 & 1 & -1 & -1 \\ -\frac{w_1}{\lambda_1} & \frac{w_1}{\lambda_1} & -\frac{w_2}{\lambda_2} & \frac{w_2}{\lambda_2} & -\frac{w_3}{\lambda_3} & \frac{w_3}{\lambda_3} \\ 0 & 0 & 0 & 0 & 0 & 1 \\ 0 & 0 & -e^{-\lambda^2 L_2} & e^{\lambda^2 L_2} & 0 & 0 \\ e^{-\lambda_1 L_1} & e^{\lambda_1 L_1} & 0 & 0 & 0 & 0 \end{bmatrix} \cdot \begin{bmatrix} \alpha_1 \\ \beta 1 \\ \alpha_2 \\ \beta 2 \\ \alpha_3 \\ \beta_3 \end{bmatrix} = \begin{bmatrix} 0 \\ 0 \\ 0 \\ 0 \\ 0 \\ A \end{bmatrix} \tag{2.13}$$

The solution of this system gives us the coefficients that we are looking for, and with these we can construct the solution for $\boldsymbol{\eta}_1$, $\boldsymbol{\eta}_2$ and $\boldsymbol{\eta}_3$.

Similar to $\boldsymbol{\eta}$, we can construct a solution for $\boldsymbol{\phi}$. We will do this by using the following structure

$$\boldsymbol{\phi} = \boldsymbol{\phi}_0 + \boldsymbol{\phi}_1(x)e^{i\omega t}. \tag{2.14}$$

Hereby, $\boldsymbol{\phi}_0$ is the tidally averaged flow and $\boldsymbol{\phi}_1(x)e^{i\omega t}$ is the flow caused by the tide. We can use equation (2.1) or (2.2) to relate the coefficients of $\boldsymbol{\phi}$ to those of $\boldsymbol{\eta}$. This leads to

$$\boldsymbol{\phi}_1(x) = \frac{w\omega i}{\lambda}\left(\alpha e^{-\lambda x} - \beta e^{\lambda x}\right). \tag{2.15}$$

The final solution of η and ϕ is then the real part of $\boldsymbol{\eta}$ and $\boldsymbol{\phi}$.

2.3. Salt transport

Now we have a way to describe the water flow as a function of time and location, we can begin modelling the salt transport in the channels. To do this we start off with a salt balance[4], where we denote the salt concentration as $s(x,t)$. The change in concentration (l.h.s.) consists of an advection term caused by the flow ($v = \frac{\phi}{wh}$) and an effective dispersion term. Especially this last term needs some explanation. Due to the reduction of the 3D geometry to a 1D model we have modelled the flow to be only dependent on x, while in fact there are velocity differences in the flow in the width and depth dimensions. This concept is shown in figure 2.3. This together with the effects of mixing due to turbulence is captured in the effective dispersion coefficient $\mathbb{D}$. This constant is determined empirically and can also capture other effects of order $\frac{\partial^2 s}{\partial x^2}$. Its value typically ranges from order 10^1 to 10^3 $\mathrm{m^2 s^{-1}}$ [8]. This balance can be written as,

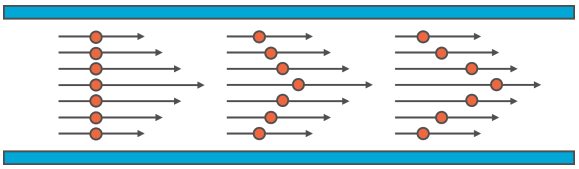

Figure 2.3: Dispersion due to velocity differences. The salt concentration is represented by the purple dots. Image inspired on the lecture notes of Environmental Physics (AP3141).

$$\frac{\partial s}{\partial t} = -v\frac{\partial s}{\partial x} + \mathbb{D}\frac{\partial^2 s}{\partial x^2}. \tag{2.16}$$

2.3.1. Single Channel

We will now proceed with solving equation (2.16) for a single channel. We start off with describing the two boundary conditions for the single channel

At $x = 0$ (sea side) we assume that the salt concentration is constant. This means that we assume that the brackish water from the river does not lower the salt concentration because the sea is massive and is well mixed. The boundary condition at the other end is a bit more tricky. The first choice that comes to mind is the condition that as $x \to \infty$ we must have that $s(x,t) \to 0$. However, since we use a numerical approximation we need a finite domain. We can therefore approximate this boundary condition by using a large enough domain so that we can say that the concentration is zero at that end of the domain. Therefore the two boundary conditions are:

$$\begin{aligned} s(0,t) &= s_* \\ s(L,t) &= 0 \end{aligned} \tag{2.17}$$

To solve this equation we make two important remarks. (1) Since ϕ oscillates with an angular frequency of ω and ϕ causes a transport of salt, it follows from equation (2.16) that s will oscillate with an angular frequency of ω or a multiple of it as well. (2) The higher the multiple of ω, the smaller the amplitude of this frequency. Using only the frequencies $(-2\omega, \dots, 2\omega)$, this translates in the following Ansatz:

$$s(x,t) = \sum_{k=-2}^{2} s_k(x) e^{ki\omega t} \tag{2.18}$$

The next step is to use this Ansatz in equation (2.16) and matching the terms with the same frequency $(-2\omega, \dots, 2\omega)$. Note that we ignore the terms for -3ω and 3ω, since we assume their contribution to the overall solution are small. The matching of these 5 frequencies lead to 5 equations. If we define $\vec{s}$ as:

$$\vec{s} = \begin{bmatrix} s_{-2} \\ s_{-1} \\ s_0 \\ s_1 \\ s_2 \end{bmatrix} \tag{2.19}$$

Then we can write the 5 equations as:

$$\mathbf{A}\vec{s} + \mathbf{B}(x)\frac{\partial \vec{s}}{\partial x} + \mathbf{C}\frac{\partial^2 \vec{s}}{\partial x^2} = \vec{0} \tag{2.20}$$

with matrices $\mathbf{A}$, $\mathbf{B}$ and $\mathbf{C}$ defined below:

$$\begin{aligned}
\mathbf{A} &= \begin{bmatrix} -2i\omega & 0 & 0 & 0 & 0 \\ 0 & -1i\omega & 0 & 0 & 0 \\ 0 & 0 & 0 & 0 & 0 \\ 0 & 0 & 0 & i\omega & 0 \\ 0 & 0 & 0 & 0 & 2i\omega \end{bmatrix} \\
\mathbf{B} &= \frac{1}{2wh}\begin{bmatrix} \overline{\boldsymbol{\phi}_0} + \boldsymbol{\phi}_0 & \overline{\boldsymbol{\phi}_1} & 0 & 0 & 0 \\ \boldsymbol{\phi}_1 & \overline{\boldsymbol{\phi}_0} + \boldsymbol{\phi}_0 & \overline{\boldsymbol{\phi}_1} & 0 & 0 \\ 0 & \boldsymbol{\phi}_1 & \overline{\boldsymbol{\phi}_0} + \boldsymbol{\phi}_0 & \overline{\boldsymbol{\phi}_1} & 0 \\ 0 & 0 & \boldsymbol{\phi}_1 & \overline{\boldsymbol{\phi}_0} + \boldsymbol{\phi}_0 & \overline{\boldsymbol{\phi}_1} \\ 0 & 0 & 0 & \boldsymbol{\phi}_1 & \overline{\boldsymbol{\phi}_0} + \boldsymbol{\phi}_0 \end{bmatrix} \\
\mathbf{C} &= \begin{bmatrix} -\mathbb{D} & 0 & 0 & 0 & 0 \\ 0 & -\mathbb{D} & 0 & 0 & 0 \\ 0 & 0 & -\mathbb{D} & 0 & 0 \\ 0 & 0 & 0 & -\mathbb{D} & 0 \\ 0 & 0 & 0 & 0 & -\mathbb{D} \end{bmatrix}
\end{aligned} \tag{2.21}$$

This system (2.20) is hard to solve analytically because $\mathbf{B}$ is dependent on x via $\boldsymbol{\phi}_1$. Therefore we will numerically solve this system in the spatial dimension. For the first derivative backward difference is used and for the second derivative the second-order central difference method is used. This can be written as

$$\begin{aligned}
\frac{\partial \vec{s}}{\partial x} &\approx \frac{\vec{s}(x+\Delta x) - \vec{s}(x)}{\Delta x}, \\
\frac{\partial^2 \vec{s}}{\partial x^2} &\approx \frac{\vec{s}(x+\Delta x) - 2\vec{s}(x) + \vec{s}(x-\Delta x)}{\Delta x^2}.
\end{aligned} \tag{2.22}$$

The reason backward difference is used instead of the central difference for the first derivative is because otherwise the numerical system will show numerical oscillations due to the loose coupling of even and odd points.

Combining all of this with the boundary conditions (2.17) gives rise to a block matrix. The solution of this system gives us the vector $\vec{s}$ at each point in the discretized spatial domain. If we take the dot product of this vector with the time vector $[e^{-2i\omega t}, \dots, e^{2i\omega t}]^T$ we get the solution we are searching for at this coordinate for every point in time.

2.3.2. Branched Channels

Now we know how to solve a single channel, we are ready to extend this solution to multiple channels. The governing equation for any channel in this system is still equation (2.16), and we still use the geometry as sketched in figure (2.2).

We will start with the boundary conditions at the junction. To simplify the notation we will denote the transport (the advection term plus the diffusion term) as T. The boundary condition at the junction are equal concentration for all three channels (a & b) and conservation of salt mass (transport) at the junction (c). This can be written as,

$$\begin{cases} s_1(0,t) = s_2(0,t) & \text{(2.23a)} \\ s_2(0,t) = s_3(0,t) & \text{(2.23b)} \\ T_1(0,t) + T_2(0,t) + T_3(0,t) = 0. & \text{(2.23c)} \end{cases}$$

For the sea side boundary we again prescribe that there is a constant concentration (d). In the side channel there is a weir on the boundary which discharges a constant flow (ϕ_0) of freshwater (not

containing salt) into the river, and no salt can be transported past this boundary. This results in a no-transport condition (e). The boundary condition of the main channel is similar to that of the single channel. We would like that as $x \to \infty$ we have that $s(x,t) \to 0$. We approximate this by using a large enough domain so that we can say that the concentration is zero at that end of the domain. We use L_3 to denote the length of the numerical domain. (f).

$$\begin{cases} s_1(0,t) = s_0 & \text{(2.23d)} \\ T_2(L_2,t) = 0 & \text{(2.23e)} \\ s_3(L_3,t) = 0 & \text{(2.23f)} \end{cases}$$

We will now continue with solving for the salt concentration. We can use most of the analysis of the single channel as we understand that, other than the boundary conditions, each channel will still behave as described in section 2.3.1. We can therefore reuse the matrices for each of the channels interior points and only have to think about the boundary conditions. We define $\mathbf{M}_1$ for the sea channels' interior points, $\mathbf{M}_2$ for the side channels' interior points and $\mathbf{M}_3$ for the main channels' interior points. We can summarize these equations in the following block matrix. The components of this matrix are other matrices which in turn consist of other matrices. n denotes the number of frequencies used, in our analysis we use $n = 5$ as described in equation (2.18).

$$\begin{bmatrix} \mathbf{M}_1 & \mathbf{0}_{n\cdot(m_1-2),n\cdot m_2} & \mathbf{0}_{n\cdot(m_1-2),n\cdot m_3} \\ \mathbf{0}_{n\cdot(m_2-2),n\cdot m_1} & \mathbf{M}_2 & \mathbf{0}_{n\cdot(m_2-2),n\cdot m_3} \\ \mathbf{0}_{n\cdot(m_3-2),n\cdot m_1} & \mathbf{0}_{n\cdot(m_3-2),n\cdot m_2} & \mathbf{M}_3 \end{bmatrix} \begin{bmatrix} \vec{s}_1 \\ \vec{s}_2 \\ \vec{s}_3 \end{bmatrix} = \begin{bmatrix} \vec{0}_{n\cdot m_1} \\ \vec{0}_{n\cdot m_2} \\ \vec{0}_{n\cdot m_3} \end{bmatrix} \tag{2.24}$$

This corresponds to $n\cdot(m_1+m_2+m_3-6)$ equations for $n\cdot(m_1+m_2+m_3)$ unknowns (the length of the stacked vectors $\vec{s}_1$, $\vec{s}_2$ and $\vec{s}_3$). The missing $n\cdot 6$ equations are exactly the 6 boundary conditions. These boundary conditions (2.23 a-f) can be rewritten into the same form as equation (2.24). This will result in n equations per boundary condition, namely one equation for every frequency, bringing the total to the required $n\cdot(m_1+m_2+m_3)$ equations. This is worked out in more detail in the appendix. The vectors $\vec{s}_1$, $\vec{s}_2$ and $\vec{s}_3$ give us the solution at each point in the domain of the channels when the dot product is taken with the time vector $[e^{-2i\omega t}, \dots, e^{2i\omega t}]^T$. We have an analytical solution in the time domain and a numerical solution in the spatial domain.

2.4. Analysis methods

2.4.1. Characteristic length and concentration

To get a feel for equation (2.16) we can try to analyse what would happen if we do not take the tidal influences into account. We will get a steady-state solution ($\frac{\partial s}{\partial t} = 0$) since there is no part any more that varies with time, and $v(x,t) = \frac{\phi}{wh}$ reduces to a constant ($\frac{\phi_0}{wh}$), namely the tidally averaged flow velocity. The solution of this (constant coefficients) ordinary differential equation, taking the boundary conditions as described before into account, is given by:

$$s = s_* e^{-\frac{\phi_0}{wh\mathbb{D}}x} \tag{2.25}$$

Two important insights arise by looking at this solution. First we see that the solution exponentially decays as x increases, secondly we see that the initial concentration at the sea (s_0) does not influence the behaviour of the solution, but only scales it. These two insights lead us to define a characteristic length and a characteristic concentration.

For the characteristic concentration we can use s_*. Now we can define the dimensionless concentration $\hat{s} = s/s_*$, note that dimensionless symbols will be indicated by a hat. For the characteristic length we take the point of the solution where the concentration at that distance is only 10% of the initial concentration. This means that we define L to be:

$$L = \frac{wh\mathbb{D}}{\phi_0} ln(0.1) \tag{2.26}$$

This leads to the following dimensionless variables:

$$\begin{cases} \hat{s} = \dfrac{s}{s_*} & \text{(2.27a)} \\ \hat{x} = \dfrac{x}{L} & \text{(2.27b)} \end{cases}$$

2.4.2. Scaling

To further improve our understanding of the salt dynamics we can use scaling to look at the magnitude of the different processes that influence the salt balance. We are particularly interested in the tidally-averaged salt concentration. This corresponds to the s_0 term in equation (2.18). If we look at equation (2.20), and only focus on the s_0 term, we can see the terms that influence it.

We use the characteristic length and concentration as defined above (2.27) to rewrite this equation into dimensionless variables.

$$\frac{1}{2\phi_0}\left(\phi_1\frac{\partial\hat{s}_{-1}}{\partial\hat{x}} + \overline{\phi_1}\frac{\partial\hat{s}_1}{\partial\hat{x}}\right) + \frac{\partial\hat{s}_0}{\partial\hat{x}} - \frac{1}{ln(0.1)}\frac{\partial^2\hat{s}_0}{\partial\hat{x}^2} = 0 \tag{2.28}$$

To use scaling to assess the importance of each of the terms we have to keep in mind that the above equation is still complex. This is especially of importance in the first term. If we consider the polar form of ϕ_1 and $\frac{\partial\hat{s}_1^*}{\partial\hat{x}}$, we see that the real part of their multiplication is,

$$\mathbb{R}\mathrm{e}\left\{\overline{\phi_1}\frac{\partial\hat{s}_1}{\partial\hat{x}}\right\} = |\phi_1| \cdot \left|\frac{\partial\hat{s}_1}{\partial\hat{x}}\right| \cdot \cos\left(\Delta\varphi_{\phi,s_1}\right) \tag{2.29}$$

Here $\Delta\varphi_{\phi,s_1}$ denotes the phase difference between ϕ_1 and $\frac{\partial\hat{s}_1}{\partial\hat{x}}$. A similar argument can be made for ϕ_1 and $\frac{\partial\hat{s}_{-1}}{\partial\hat{x}}$, with the same phase difference $\Delta\varphi_{\phi,s_1}$.

3

Results

In this chapter, we first present and discuss the results obtained from the wave equation (tidal flow and water height). An insight of the underlying flow behaviour is needed for our understanding of the salt transport, which will be presented in the subsequent section. We will need to choose some values to use in the model, the chosen values are shown in table 3.1. These values are used consistently throughout the results, to ensure a fair comparison. In the branched channel situation, every branch uses these same values as the single channel unless clearly indicated otherwise. The number of grid points used in the sea- and main channel is 1800. The number of grid points in the side channel varies with the length L_2, but the same distance between the grid points is used as in the main channel which is $\Delta x = 100\mathrm{m}$. For the single channel and branched channels a doubling of the number of grid-points gave no visible better resolution.

w	$2 \cdot 10^2 \mathrm{m}$
h	$1 \cdot 10^1 \mathrm{m}$
c_d	$1 \cdot 10^{-2}$
U	$1 \mathrm{m\,s^{-1}}$
ω	$1.405 \cdot 10^{-4} \mathrm{rad\,s^{-1}}$
ϕ_0	$-1 \cdot 10^2 \mathrm{rad\,s^{-1}}$

Table 3.1: The model settings to be used throughout the whole chapter.

3.1. Flow behaviour

We will first look at the results of the single semi-infinite channel, afterwards we will present the effect of the addition of a second channel.

3.1.1. Semi-Infinite Channel

From our analytic solution (2.9) we can already notice two important properties. We see that due to the sine function there will be oscillations both in space (x) and time (t). Furthermore, we see that the wave height (and therefore also the flow) decreases exponentially as x becomes larger. This decay is due to the dissipation of energy due to friction. These are of course two properties that we would expect. Furthermore if we were to ignore the decay, we would expect there to be characteristics over which the solution should stay constant [3]. This should be at the wave velocity including friction, which is $c' = \frac{\omega}{\lambda(\omega)}$. Lastly, if we take $x = 0$ (the sea boundary) we see that the solution indeed follows the boundary condition.

In figure (3.1) the results for a semi-infinite channel with a default set of parameters are plotted. The plot shows iso-value contours of the change in water height (η) and the velocity of the water (v). For η, red indicates an elevation and blue a decrease in water height. For ϕ a positive flow (landward) is red and a negative flow (seaward) is blue. The wave velocity is indicated with a black arrow, we see that along this arrow the solution does not oscillate but decays exponentially.

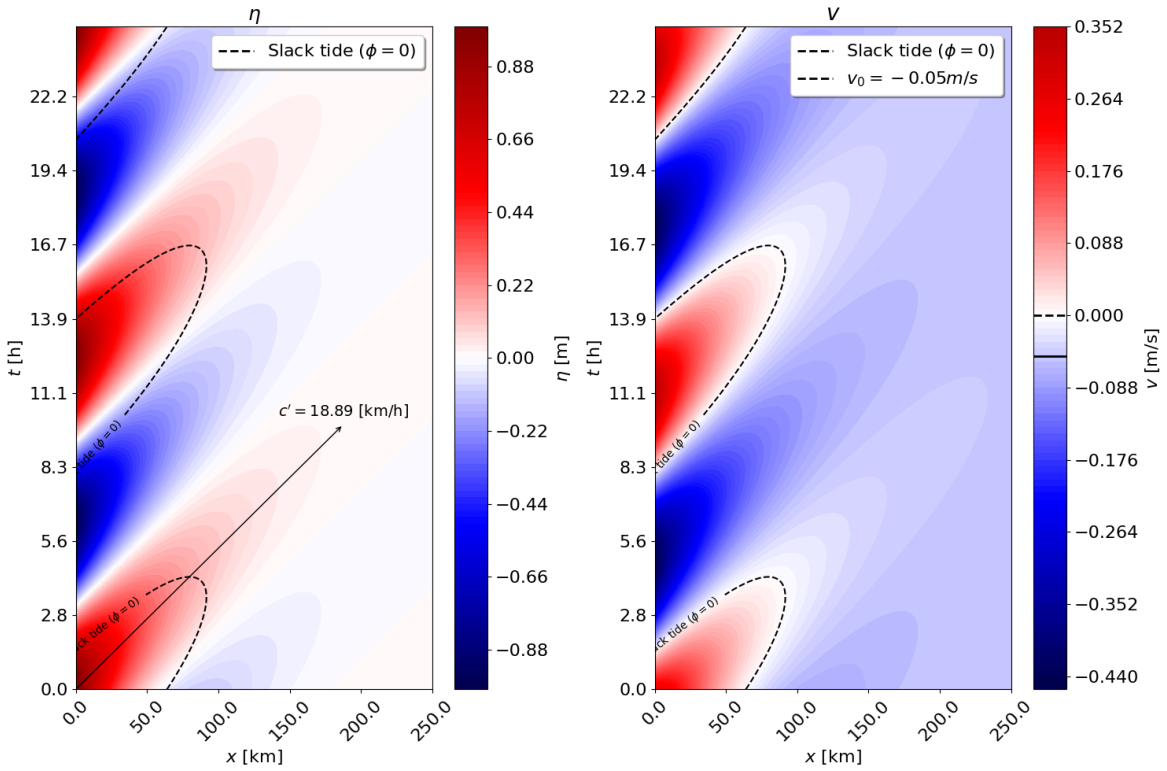

Figure 3.1: Water height η and flow velocity $v = \frac{\phi}{wh}$ due to tidal influences in a semi-infinite channel (constant width and depth). Water height $\eta = 0$ and flow $\phi = 0$ are represented in white. The tidally averaged velocity v_0 is shown as a black line on the colorscale. The wave velocity including friction is indicated with an arrow.

In figure 3.2 a few slices of η and ϕ in the spatial and temporal direction are given. In the above two plots we see a slice in time taken at different x points. We clearly see the oscillations of the solution and we see the amplitude of the oscillating decreasing with increasing x. In the two plots at the bottom we see a slice taken in space (x) at different moments in time (t). In this plot the exponential decay is more noticeable. We see clearly that the wave dampens out as $x \to \infty$.

Since ϕ is a superposition of the tidal influenced part and the average flow part (which is negative), the negative flow (seaward) is dominant over the positive flow (landward). This can be noticed in figure 3.1 by the velocity (v) plot being mostly blue. Moreover note the slack tide ($\phi = 0$) in the plot, these are the moments in which the flow in the river reverses direction, flowing landward instead of seaward. This aspect will become important later on with the analysis of the salt intrusion.

3.1.2. Branched Channels

We will now continue with the branched channel situation, of which the geometry is shown in figure (2.2). The same parameters as in the semi-infinite channel are used, with the addition of a second channel of length $L_2 = 40\text{km}$ at the location $L_1 = 25\text{km}$. All the other properties are the same as the other two channels. The results for the water height are given in figure (3.3) and the results for the flow are given in figure (3.4). From looking at the analytical solution we again expect there to be oscillations both in space and time with an exponential decay. However, there are now differences due to reflections in the side channel.

Figure 3.3 shows the results for the water height (η). We see that the wave from the tidal forcing propagates in the system. An important thing to notice is that due to the no-flow boundary condition at the end of the side channel the incoming wave is reflected at this boundary and 'moves back' into the sea channel again. Two characteristics are indicated with arrows in the side channel. In the sea channel and the side channel we see a wave interference effect caused by the reflections. Instead of the neat diagonal iso-contours, as in the main channel, we see a more complex warped shape. In figure 3.3 this is most clear in the sea channel. If the reflected tide wave returns when an incoming

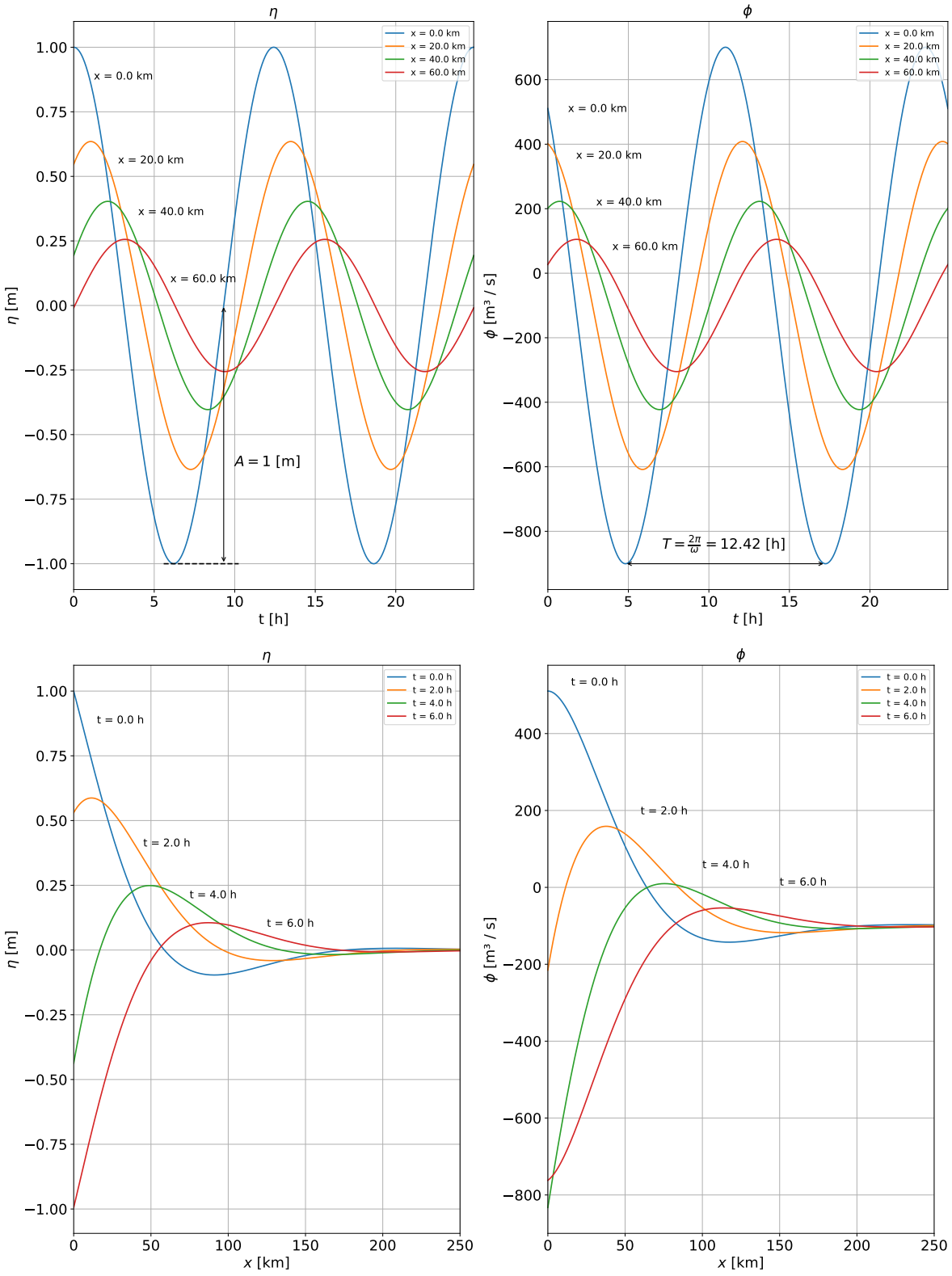

Figure 3.2: Slices of η and ϕ taken in x and t. The above two plots are slices taken in the time domain and the two slices below are taken in the spatial domain. All for the single semi-infinite channel.

ebb wave enters, the tidal amplitude is damped. In the main channel there are no reflections. The tidal wave propagates until it has completely dissipated.

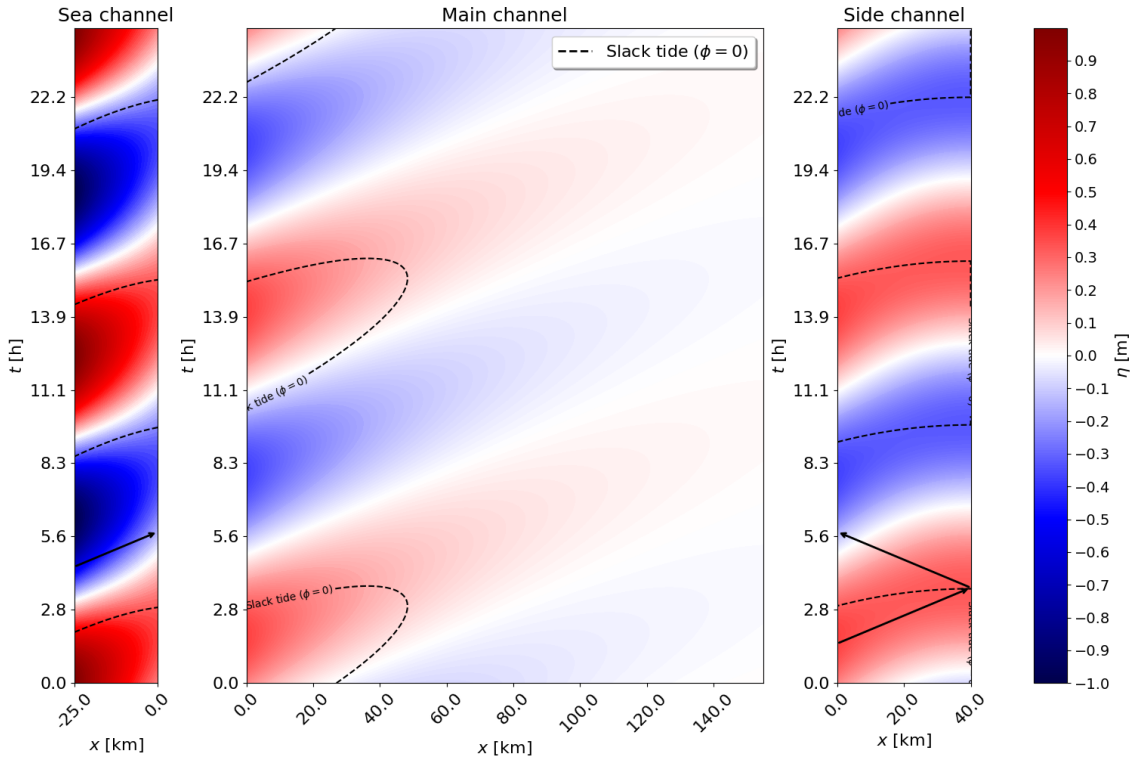

Figure 3.3: Water height η due to tidal influences in a branched channel system. Water height $\eta = 0$ is represented in white, and the contours of the slack tide (black dashed lines) are shown as well. The arrows show a reflection in the side channel and the interference with a new tidal wave at the junction.

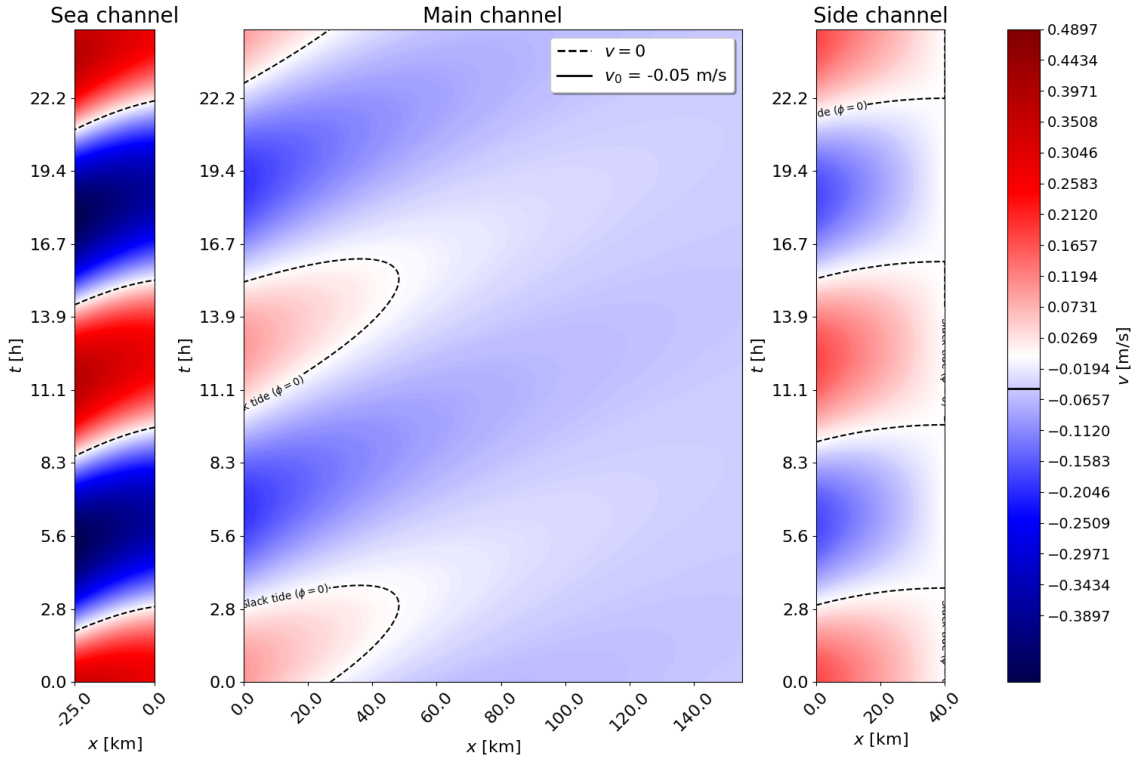

Figure 3.4: Water flow $v = \frac{\phi}{wh}$ due to tidal influences in a branched channel system. Flow $\phi = 0$ is represented in white. The tidally averaged flow velocity is indicated as a black line in the colorscale.

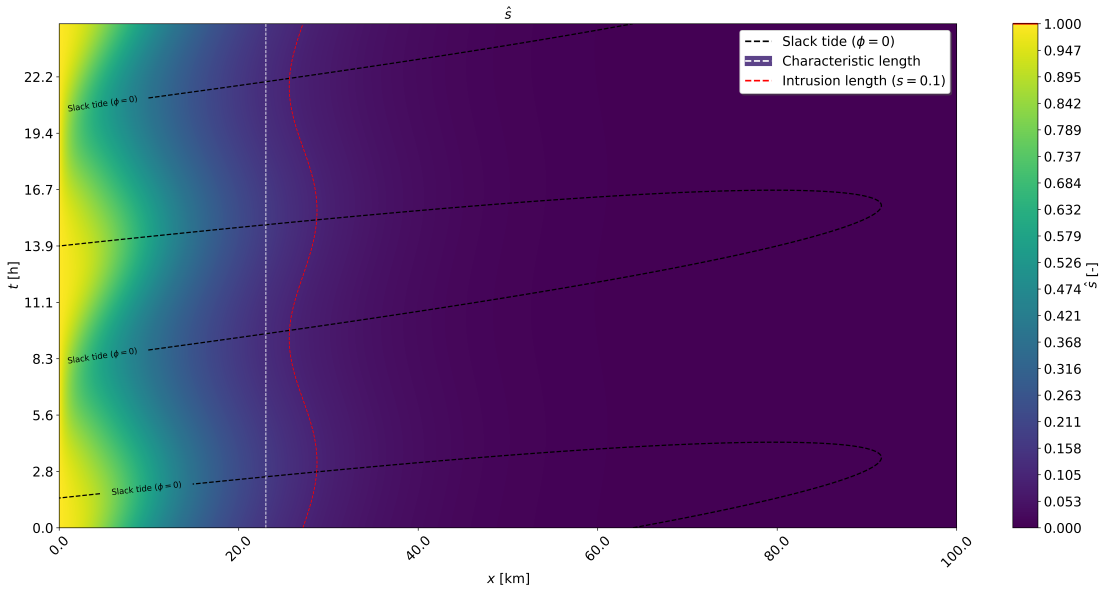

Figure 3.5: The scaled salt concentration $\hat{s}$ in the single semi-infinite channel.

In figure (3.4) the results for the corresponding flow (ϕ) are displayed. As with the single semi-infinite channel, the flow is a superposition of the average flow with the tidal influenced flow, and therefore we see more seaward flow (blue) than landward flow (red) in the sea- and main channel.

In the side channel the situation is different. Since there is a no-flow condition at the end, the mass transport of this channel should be balanced. The mass transport in equals the mass transport out over a tidal period, as there is no net transport in the long term. This is indeed what we see in the figure. Again we can also see an interference effect of the waves in the sea- and side channel.

3.2. Salt intrusion

In this section we will explore the results of the salt model. We will first look at a single channel, then a specific configuration with a branched channel to get an understanding for the system dynamics. Finally, we will see how the salt intrusion changes as we vary the distance to the junction (L_1) and the length of the channel (L_2).

3.2.1. Semi-Infinite Channel

In figure 3.5 the results for a single semi-infinite channel are plotted. We see the salt concentration decreasing rapidly as x becomes larger. In fact, this decrease is almost exponential as described by the solution of the problem without tide (2.25). The 10% concentration contour is also plotted (in red), and we see that this is close to the characteristic length L which is represented as a white dashed line, but slightly more landwards. This means that the salt intrusion is slightly larger due to tide compared to the solution without tide.

This can be explained by looking at the scaled equation (2.28) of section 2.4.2. If we look at the coefficients of the tidally averaged advection term and the dispersion term, we see that their magnitudes in this situation are 1 and $1/ln(10) \approx 0.43$. The coefficient in front of the tidally influenced part is a bit more tricky to analyse. This is due to the phase difference between $\frac{\partial \hat{s}_{-1}}{\partial \hat{x}}$ or $\frac{\partial \hat{s}_1}{\partial \hat{x}}$ and ϕ_1. They are almost completely out of phase with each other which makes this prefactor relatively small. That they are out of phase with each other can be seen in figure 3.5. The salt is at its maximum during the slack tide. Therefore when the change in salt concentration in time is around zero, the change of flow in time is highest. This indicates that they are almost completely out of phase.

We can also see that there is an oscillating behaviour with the same frequency of the tide, but the double frequency of the tide is not noticeable in the plot. This is also one of the assumptions that we made while building the salt model. This is more noticeable if we split up the contributions of the different frequencies, this is done in figure (3.6). We see that the most part comes from the constant

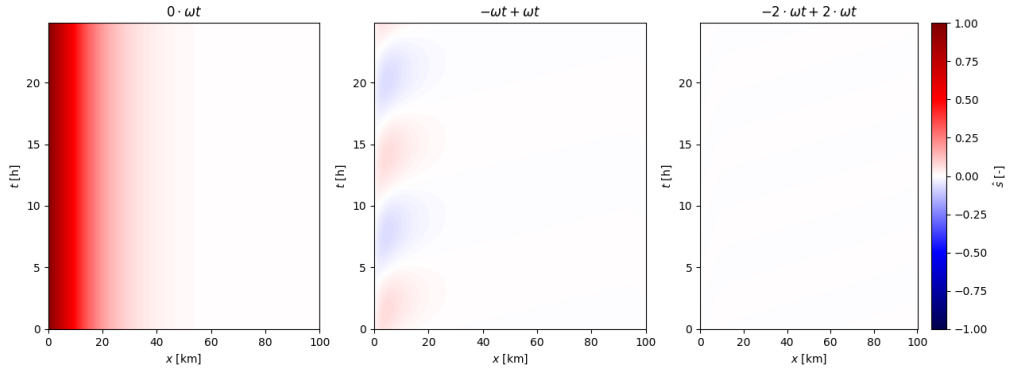

Figure 3.6: The influence of the different frequencies on the salt concentration. The actual concentration is the sum of all of these. The negative and positive frequencies ($-\omega t$ and ωt) are combined.

part, there is a slight contribution from the ωt part, and the contribution of the $2\omega t$ part is not noticeable.

The contours of the slack tide ($\phi = 0$) are also plotted. We can notice that there is a minimum or a maximum in the salt concentration at this contour. This can be explained if we consider the underlying process. The moment the flow in the channel reverses, salt is transported by advection landwards. This means that the salt concentration is building up. The moment the flow reverses again, and water is streaming into the sea, the salt is transported by advection seawards and the concentration decreases again.

3.2.2. Branched Channels

Before we will continue with the analysis of the effect of changing the junction location (L_1) and the branch length (L_2) we will have a look at a specific example. Figure 3.7 shows the salt concentration in the branched channel situation. We notice almost the same features as described above in the main- and sea channel. We see the decrease in concentration, the oscillating behaviour and the maximum and minimum at slack tide. In the side channel we see an almost constant concentration. This can be explained by the absence of tidally averaged flow in the channel. There is no fresh water flow in that channel to flush out the salt water so the concentration in the channel will be roughly the average concentration at the junction except for a small tidal influence.

3.2.3. Effect junction location and branch length

In this section, we will present the results of varying the location of the junction and the length of the branch and explore how this affects salt intrusion in a tidal system. We will compare the salt intrusion length in the branched system to that of the single channel. Therefore we will work with the difference in intrusion length between the two.

In figure 3.8 we see the difference in salt intrusion length if we vary L_1 (the length between the sea and the junction) and L_2 (the length of the branched channel) compared to the semi-infinite channel. It is plotted for different effective dispersion coefficients, but all with a tidally averaged flow of $\phi_0 = -100\mathrm{m}^3\,\mathrm{s}^{-1}$.

We see that as L_1 increases (the junction point is located further inland) the effect on the salt intrusion decreases. The dissipation of energy due to friction can explain this relation. If the junction is further inland, the energy of the tidal wave has mostly been dissipated before it has reached the junction. This can be seen by looking at the flow behaviour of the branched channel. Therefore the branch does not cause a different flow behaviour for the part of the channel that the salt can reach and consequently the salt intrusion is not influenced by the branch. Although in the figure L_1 is not large enough for the difference in salt intrusion to go to zero, it is checked for several configurations that the difference indeed goes to zero.

In figure 3.9 we see the difference in intrusion length but now for $\phi_0 = -50\mathrm{m}^3\,\mathrm{s}^{-1}$. Something that immediately stands out is the large blue area. This means that for those configurations of L_1 and L_2 the salt intrusion length is decreased by adding a branching channel. We see that this decrease is around $L_2 = 60\mathrm{km}$.

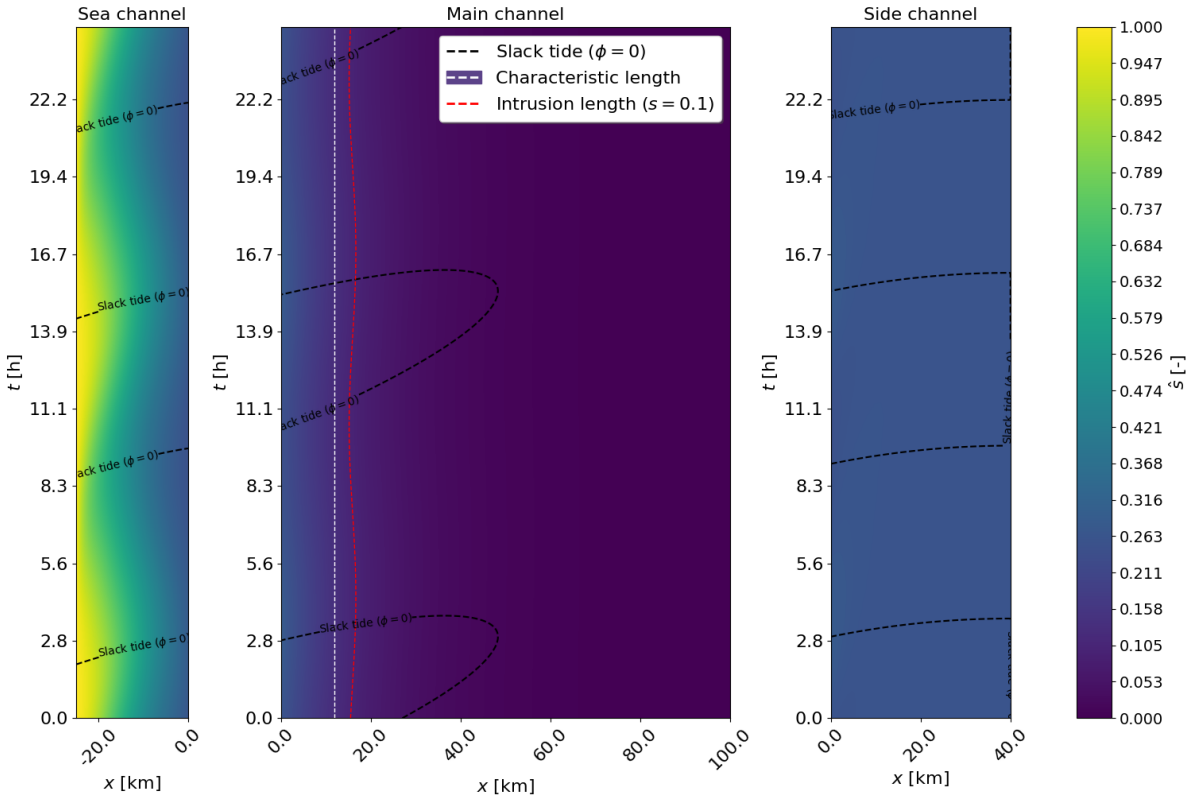

Figure 3.7: The scaled salt concentration for a specific configuration of the branched channel system.

This decrease can be explained if we look at the wave velocity including friction ($c' = 18.89\mathrm{km\,h^{-1}}$) we can calculate the wave length $\lambda = c'T = 234.61km$. This means that a quarter wavelength is $\frac{\lambda}{4} = 58.7km$, which coincides with the peak we see in the data. To understand this a bit better, we can take a look at what happens with the flow pattern in a side channel without friction with a quarter wavelength. Note that in this case the wavelength is larger due to the absence of friction. This flow pattern is shown in figure 3.10. We see that in this situation that only in the sea channel and the side channel tidal flow occurs . If we go back to our situation including friction, we would still expect this destructive interference, however due to friction we do not expect a full cancellation but only a damping of the tidal waves.

Another feature that is noticeable, is the peak in salt intrusion difference arising at $L_1 = 10\mathrm{km}$. The location seems independent of the effective dispersion coefficient $\mathbb{D}$ and the tidally averaged flow ϕ_0. The height of the peak does seem to be influenced by the effective dispersion coefficient $\mathbb{D}$, where a lower coefficient leads to a larger difference in intrusion length.

This reason why the negative valley exists for $\phi_0 = -50\mathrm{m^3\,s^{-1}}$ and not for $\phi_0 = -100\mathrm{m^3\,s^{-1}}$ might be due to that in the first case the 'pressure' of the freshwater pushing the salt water back is weaker. In this case the intrusion length can be further than the junction. If due to the interference the flow is weakened in the main channel of the branched situation then the intrusion length will be reduced compared to the single channel situation. However in this case you would still expect the valley to be visible for smaller values of L_1, nevertheless it might be that this effect is outbalance by the peak the exists for small values of L_1.

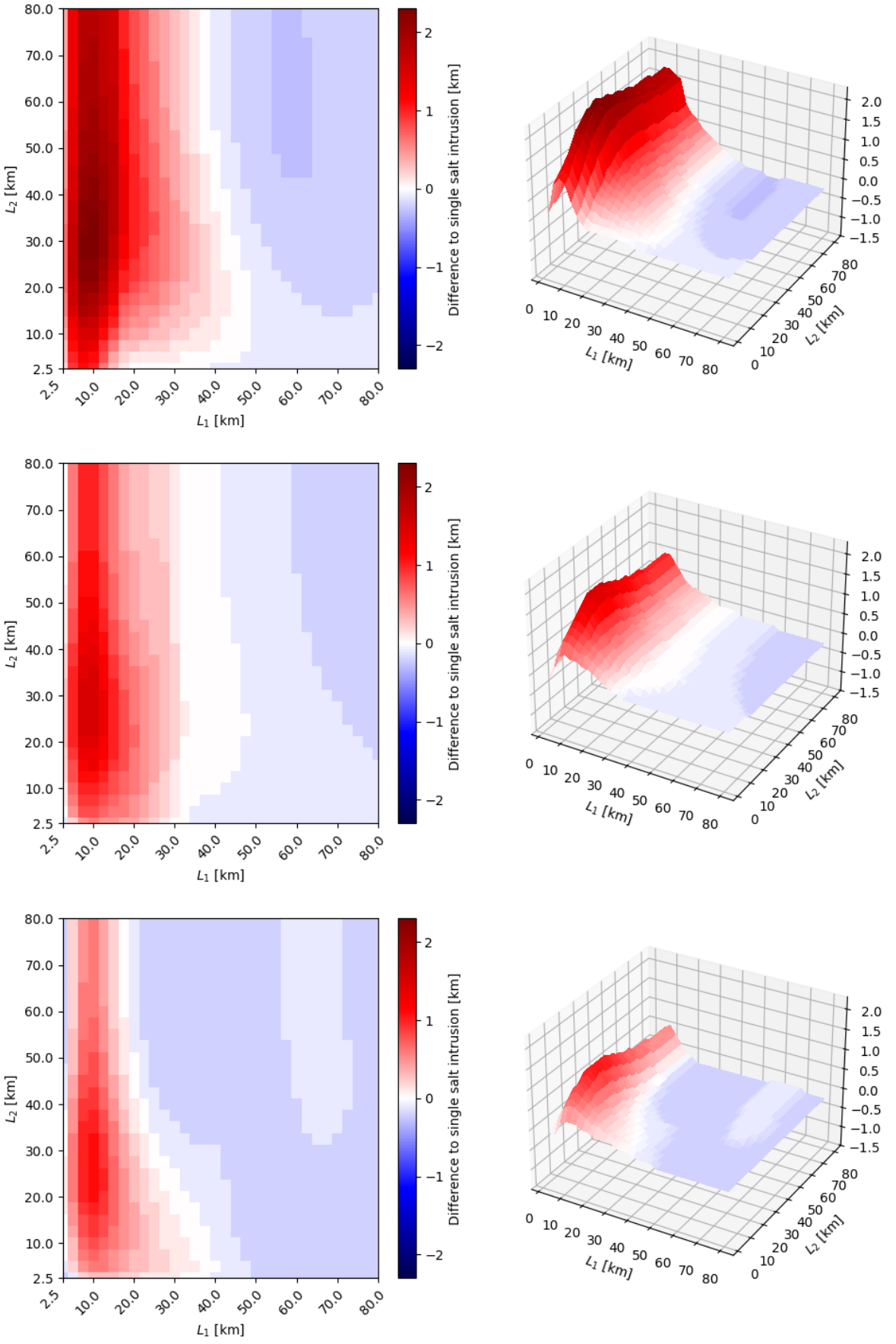

Figure 3.8: The difference of salt intrusion lengths compared to the single channel. This is plotted for different effective dispersion coefficients all using the same tidally averaged flow $\phi_0 = -100\mathrm{m}^3\,\mathrm{s}^{-1}$. The dispersion coefficients from top to bottom are: $\mathbb{D} = 200, 500, 800\mathrm{m}^2\,\mathrm{s}^{-1}$.

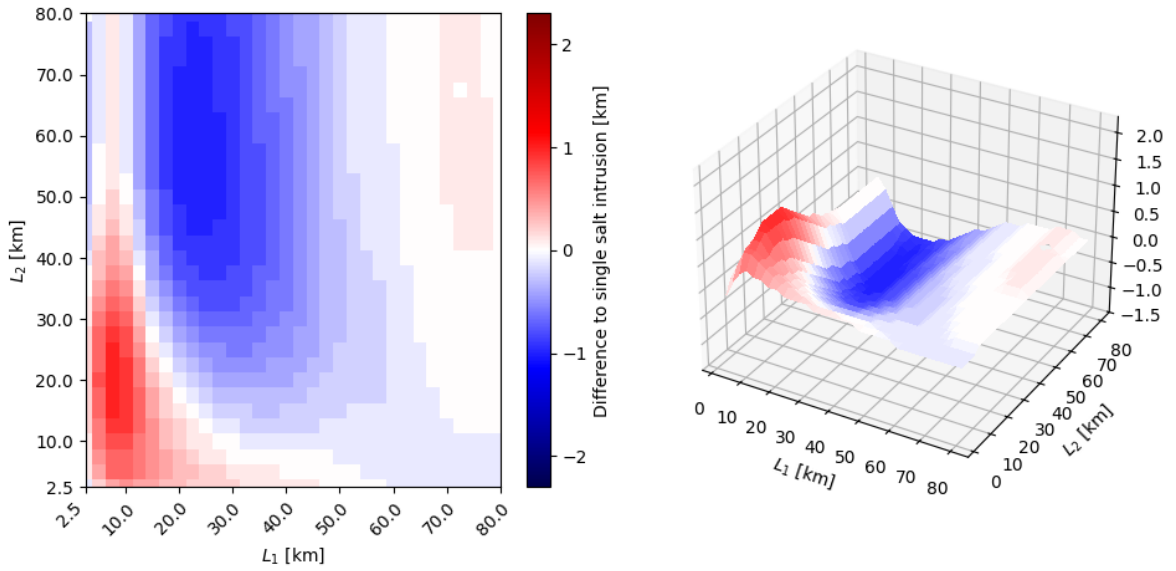

Figure 3.9: The difference of salt intrusion lengths compared to the single channel. This is plotted for a system with an effective dispersion coefficient of $\mathbb{D} = 500\mathrm{m}^2\ \mathrm{s}^{-1}$ and a tidally averaged flow of $\phi_0 = -50\mathrm{m}^3\ \mathrm{s}^{-1}$.

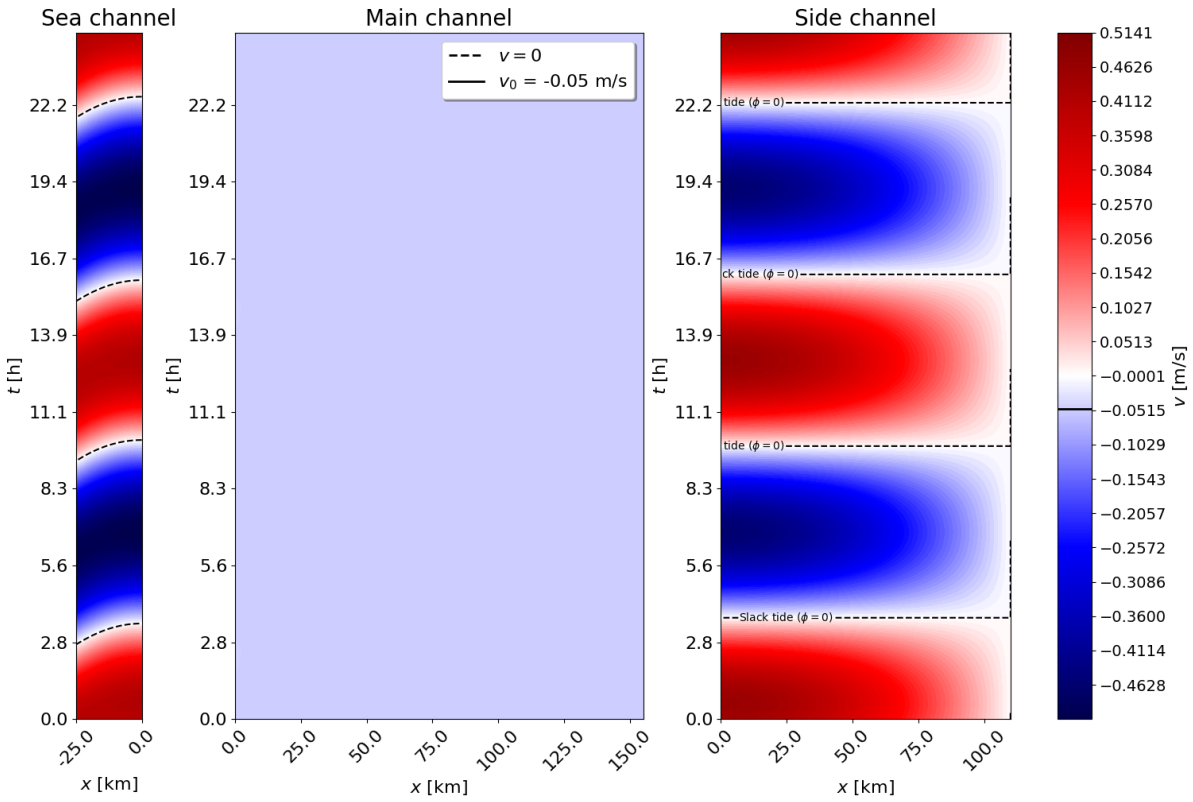

Figure 3.10: The flow behaviour in a branched channel system with no friction in the side channel. The side channel is exactly a quarter of the wavelength.

4

Conclusion

The aim of this thesis was to investigate the effect of a finite-length side channel on the salt intrusion in a semi-infinite main channel. To reach this goal we had to develop a simple exploratory model for the flow and salt intrusion due to tidal influences in estuarine environments. The focus was on the effect of the length of the side channel and the distance of the junction to the sea. The model was developed by considering a channel of constant width, depth and friction factor. Conservation of mass and conservation of momentum were used to derive a wave equation including a friction term.

After the flow behaviour was solved analytically, the model was extended by including a salt balance. The salt balance assumes the channels to be perfectly mixed in the vertical direction. This equation was solved analytically in the time domain and for the spatial part a numerical model was created to solve for the salt concentration.

4.1. Main findings

For the chosen model parameters, the intrusion length for a single channel can be approximated well by considering a characteristic length defined by solving the salt balance without the tidally dependent part. It is observed that a maximum and minimum in the salt concentration occurs at slack tide (the moment the flow reverses direction).

In a branched system it is noticed that due to reflections of the tidal wave, interference creates a change in the flow pattern which in turn changes the salt intrusion. It is observed that, due to the zero tidally averaged flow, the salt concentration in the channel will be roughly the average concentration at the junction. This is because of the absence of fresh water discharge to flush out the salt.

The intrusion length for different configurations of a branched system was compared to that of the single channel system. For the situation analysed as described in the beginning of the results chapter, it is shown that the addition of the branch has a small (but not negligible) effect on the intrusion length (in the order of magnitude of $1\mathrm{km}$). This effect can be either positive or negative. A negative change can be observed if the length of the branching channel is close to a quarter wavelength. Due to destructive interference the tidal forcing in the main channel can be weakened thereby reducing the intrusion length. A smaller tidally averaged flow leads to a bigger influence of the tide behaviour.

4.2. Further research

There are a lot of interesting aspects still left to investigate further. In terms of model assumptions, an improvement that could be made, so the model is closer to reality, is to make the friction factor depend quadratically on the water flow rate. Currently the model has linearised the bottom stress, while more accurately it should depend quadratically on the flow rate. This can, for example, be done by using a numerical model. Secondly, the model can be extended by allowing the channel cross-section to vary gradually. In this manner, more complex geometries can be considered. Another modification to be considered is taking the increased density of salt water into account. Currently, the model assumes the increased density of the water does not affect the flow behaviour, and that the channel is perfectly mixed in the vertical direction. One can look at a model describing the salt concentration using a two layer model or a partially mixed model.

Since the solution for the flow rate and water height are analytical, the flow behaviour can be calculated quite fast. The modelling of the salt concentration is done numerically on a grid with a constant step size. The performance and accuracy of the model could be increased by considering a finer grid near the sea and the junction and a coarser grid landwards where the variations in the salt concentration are smaller.

In terms of choices on what to study, the effect of the other physical parameters can be systematically studied, especially the effect of $\mathbb{D}$ and ϕ_0 on the salt intrusion can be interesting. Furthermore, the research can be extended by looking at the effect of adding multiple branches or changing the main channel into a finite channel, this will cause more reflections and presumably a more complex wave interference pattern. Another extension could be to take other tide components into account. The current model only focuses on the M2 tidal component, however there are many more. One can look at the addition of the S2 component (the solar influence). Since the different tidal components will propagate at different velocities in the system and have different wavelengths. This will also influence the dynamics of the system.

A

Appendix

A.1. Wave equation derivation

We start with equation (2.2) and apply the approximation as described in section 2.2.1 ($\frac{\tau}{\rho h} = \frac{r}{wh}\phi$ and neglecting $\frac{\phi}{(wh)^2}\frac{\partial \phi}{\partial x}$). Furthermore, we multiply with wh.

$$\frac{\partial \phi}{\partial t} + whg\frac{\partial \eta}{\partial x} + r\phi = 0 \tag{A.1.1}$$

The second step is to differentiate (A.1.1) in space and (2.1) in time. This leads to:

$$\frac{\partial^2 \phi}{\partial x \partial t} + whg\frac{\partial^2 \eta}{\partial x^2} + r\phi = 0 \tag{A.1.2a}$$

$$w\frac{\partial^2 \eta}{\partial t^2} = -\frac{\partial^2 \phi}{\partial t \partial x} \tag{A.1.2b}$$

We now substitute the two equations and get:

$$-w\frac{\partial^2 \eta}{\partial t^2} + whg\frac{\partial^2 \eta}{\partial x^2} + r\frac{\partial \phi}{\partial x} = 0 \tag{A.1.3}$$

The last step is to use equation (2.2) once more and to divide by $-w$.

$$\frac{\partial^2 \eta}{\partial t^2} + r\frac{\partial \eta}{\partial t} = c^2\frac{\partial^2 \eta}{\partial x^2} \tag{A.1.4}$$

With $c = \sqrt{gh}$ and this is the required wave equation as mentioned in (2.3).

A.2. Semi-Infinite channel derivation

We start by Fourier transforming the wave equation (2.3). We use the following Fourier transform:

$$\mathcal{F}\{f\}(\xi) = \frac{1}{2\pi}\int_{-\infty}^{\infty} f(\bar{x})e^{i\xi\bar{x}}d\bar{x} \tag{A.2.1a}$$

$$\mathcal{F}^{-1} = \int_{-\infty}^{\infty} \mathcal{F}(\xi)e^{-i\xi x}d\xi \tag{A.2.1b}$$

This leads to:

$$(-i\xi)^2\mathcal{F}\{\eta\} + r(-i\xi)\mathcal{F}\{\eta\} = c^2\frac{\partial^2 \mathcal{F}\{\eta\}}{\partial x^2} \tag{A.2.2}$$

So this results in an ordinary differential equation for $\mathcal{F}\{\eta\}$.

$$\frac{\partial^2 \mathcal{F}\{\eta\}}{\partial x^2} = -\frac{\xi^2 + r\xi i}{c^2}\mathcal{F}\{\eta\} \tag{A.2.3}$$

If we define $\lambda^2 = -\frac{\xi^2 + r\xi i}{c^2}$ the general solution of this equation is:

$$\begin{aligned}\mathcal{F}\{\eta\} &= c_1(\xi)e^{-\lambda x} + c_2(\xi)e^{\lambda x} \\ &= c_1(\xi)e^{\mathbb{Re}\{-\lambda\}x}e^{\mathbb{Im}\{-\lambda\}xi} + c_2(\xi)e^{\mathbb{Re}\{\lambda\}x}e^{\mathbb{Im}\{\lambda\}xi}\end{aligned} \tag{A.2.4}$$

Since we have $\mathbb{Re}\{\lambda\} = \sqrt{\frac{1}{2}}\frac{1}{c}\sqrt{-\xi^2 + \sqrt{\xi^4 + r^2\xi^2}} > 0$. We must have that $c_2(\xi) = 0$ since the solution should be bounded as $x \to \infty$ and $\exp\{\mathbb{Re}\{\lambda\}x\} \to \infty$ as $x \to \infty$. To incorporate the other boundary condition, we fourier transform this condition as well:

$$\begin{aligned}\mathcal{F}\{\eta(0,t)\} &= \mathcal{F}\{A\sin(\omega t + \theta)\} \\ &= A\frac{i}{2}\left(e^{-i\theta}\delta(\xi - \omega) - e^{i\theta}\delta(\xi + \omega)\right)\end{aligned} \tag{A.2.5}$$

And we therefore conclude that $c_1(\xi) = A\frac{i}{2}\left(e^{-i\theta}\delta(\xi - \omega) - e^{i\theta}\delta(\xi + \omega)\right)$. The next step is to do an inverse Fourier transform on the solution for $\mathcal{F}\{\eta\}$.

$$\eta = \int_{-\infty}^{\infty} A\frac{i}{2}\left(e^{-i\theta}\delta(\xi - \omega) - e^{i\theta}\delta(\xi + \omega)\right)e^{\mathbb{Re}\{-\lambda\}x}e^{\mathbb{Im}\{-\lambda\}xi}e^{-i\xi x}d\xi \tag{A.2.6}$$

If we solve this and use the observation that $\lambda(-\omega) = \overline{\lambda(\omega)}$, we get:

$$\begin{aligned}\eta(x,t) &= \frac{i}{2}e^{-\mathbb{Re}\{\lambda(\omega)\}x}2\mathbb{Im}\left\{e^{-(\mathbb{Im}\{\lambda(\omega)\}x + \omega t + \theta)i}\right\}i \\ &= Ae^{-\mathbb{Re}\{\lambda(\omega)\}x}\sin\left(\mathbb{Im}\{\lambda(\omega)\}x + \omega t + \theta\right)\end{aligned} \tag{A.2.7}$$

And this is the equation as described in (2.9).

A.3. Branched channel derivation

This sections is split into three subsections in section A.3.1 we derive a (complex) expression for η. The constants for this expression are subsequently derived in section A.3.3, lastly the (complex) expression for ϕ is derived in section A.3.2.

A.3.1. η derivation

We start with the complex wave equation:

$$\frac{\partial^2 \eta}{\partial t^2} + r\frac{\partial \eta}{\partial t} = c^2\frac{\partial^2 \eta}{\partial x^2} \tag{A.3.1}$$

We substitute the following Ansatz in equation (A.3.1)

$$\eta = \sum_{n=0}^{N} Z_n(x)e^{i\omega_n t} \tag{A.3.2}$$

This leads to:

$$\sum_{n=0}^{N}(i\omega_n)^2 Z_n(x)e^{i\omega_n t} + r\sum_{n=0}^{N}(i\omega_n)Z_n(x)e^{i\omega_n t} = c^2\sum_{n=0}^{N}\frac{\partial^2 Z_n(x)}{\partial x^2}e^{i\omega_n t}$$
$$\sum_{n=0}^{N}\frac{\partial^2 Z_n}{\partial x^2} + \frac{\omega_n^2 - r\omega_n i}{c^2}Z_n = 0 \tag{A.3.3}$$

This must be true for every n, if we now define $\lambda_{2,n} = \frac{-\omega_n^2 + r\omega_n i}{c^2}$:

$$\frac{\partial^2 Z_n}{\partial x^2} - \lambda_{2,n}Z_n = 0 \tag{A.3.4}$$

and this means that:

$$Z_n = \alpha_n e^{-\lambda_n x} + \beta_n e^{\lambda_n x} \tag{A.3.5}$$

and thus we have:

$$\eta = \sum_{n=0}^{N}\left(\alpha_n e^{-\lambda_n x} + \beta_n e^{\lambda_n x}\right)e^{i\omega_n t} \tag{A.3.6}$$

A.3.2. Φ derivation

We know Φ can be written as:

$$\Phi = \sum_{n=0}^{N} Y_n(x)e^{i\omega_n t} \tag{A.3.7}$$

Using this knowledge we can rewrite relation A.1.1:

$$\frac{\partial \Phi^i}{\partial t} + gw_i h_i\frac{\partial \eta_i}{\partial x} + r_i\Phi^i = 0$$
$$\frac{\partial \Phi^i}{\partial t} + r_i\Phi^i = -gw_i h_i\frac{\partial \eta_i}{\partial x}$$
$$\sum_{n=0}^{N}(i\omega_n + r_i)Y_{i,n}(x)e^{i\omega_n t} = -gw_i h_i\sum_{n=0}^{N}\left(-\alpha_n^i\lambda_{i,n}e^{-\lambda_{i,n}x} + \beta_n^i\lambda_{i,n}e^{\lambda_{i,n}x}\right)e^{i\omega_n t} \tag{A.3.8}$$

If we match the terms with the same frequencies we get:

$$Y_{i,n}(x) = \frac{gw_i h_i\lambda_{i,n}\left(\alpha_{i,n}e^{-\lambda_{i,n}x} - \beta_{i,n}e^{\lambda_{i,n}x}\right)}{i\omega_n + r_i} = \frac{w_i\omega_n i}{\lambda_{i,n}}\left(\alpha_{i,n}e^{-\lambda_{i,n}x} - \beta_{i,n}e^{\lambda_{i,n}x}\right) \tag{A.3.9}$$

A.3.3. Boundary conditions

Split boundary conditions

We will now continue with the boundary conditions of the branched channel situation.

We start with the split ($x = 0$) where we have the following boundary condition:

$$\begin{aligned} \eta_1(0,t) &= \eta_2(0,t) \\ \sum_{n=0}^{N} \left(\alpha_{1,n} + \beta_{1,n}\right) e^{i\omega_n t} &= \sum_{n=0}^{N} \left(\alpha_{2,n} + \beta_n^2\right) e^{i\omega_n t} \\ \sum_{n=0}^{N} \left(\alpha_{1,n} + \beta_{1,n} - \alpha_{2,n} - \beta_n^2\right) e^{i\omega_n t} &= 0 \end{aligned} \tag{A.3.10}$$

A similar calculation can be done for the second boundary condition at the split:

$$\eta_2(0,t) = \eta_3(0,t) \tag{A.3.11}$$

We can capture both these boundary conditions in matrix form:

$$\begin{bmatrix} 1 & 1 & -1 & -1 & 0 & 0 \\ 0 & 0 & 1 & 1 & -1 & -1 \end{bmatrix} \cdot \begin{bmatrix} \alpha_{1,n} \\ \beta_{1,n} \\ \alpha_{2,n} \\ \beta_{2,n} \\ \alpha_{3,n} \\ \beta_{3,n} \end{bmatrix} = \begin{bmatrix} 0 \\ 0 \end{bmatrix} \tag{A.3.12}$$

The other boundary condition at the split is:

$$\Phi_1 + \Phi_2 + \Phi_3 = 0 \tag{A.3.13}$$

We can rewrite this (A.3.13) using our expression for ϕ (A.3.7) as:

$$\sum_{n=0}^{N} (Y_{1,n}(0) + Y_{2,n}(0) + Y_{3,n}(0)) e^{i\omega_n t} = 0 \tag{A.3.14}$$

Using equation (A.3.9) for $Y_{i,n}(x)$ in the equation above leads to the following equation for α and β:

$$\begin{aligned} Y_{1,n}(0) + Y_{2,n}(0) + Y_{3,n}(0) &= 0 \\ \frac{w_1 \omega_n i}{\lambda_{1,n}} \left(\alpha_{1,n} - \beta_{1,n}\right) + \frac{w_2 \omega_n i}{\lambda_{2,n}} \left(\alpha_{2,n} - \beta_n^2\right) + \frac{w_3 \omega_n i}{\lambda_{3,n}} \left(\alpha_{3,n} - \beta_{3,n}\right) &= 0 \end{aligned} \tag{A.3.15}$$

If we divide by $\omega_n i$, we can write it in matrix-form:

$$\begin{bmatrix} -\frac{w_1}{\lambda_{1,n}} & \frac{w_1}{\lambda_{1,n}} & -\frac{w_2}{\lambda_{2,n}} & \frac{w_2}{\lambda_{2,n}} & -\frac{w_3}{\lambda_{3,n}} & \frac{w_3}{\lambda_{3,n}} \end{bmatrix} \cdot \begin{bmatrix} \alpha_{1,n} \\ \beta_{1,n} \\ \alpha_{2,n} \\ \beta_{2,n} \\ \alpha_{3,n} \\ \beta_{3,n} \end{bmatrix} = \begin{bmatrix} 0 \end{bmatrix} \tag{A.3.16}$$

Sea channel boundary condition
For the first branch (η_1) we have the following boundary condition:

$$\begin{aligned} \eta_1(L_1,t) &= \sum_{n=0}^{N} A_n e^{i\omega_n t} \\ \sum_{n=0}^{N} \left(\alpha_{1,n} \exp\{-\lambda_{1,n} L_1\} + \beta_{1,n} \exp\{\lambda_{1,n} L_1\}\right) e^{i\omega_n t} &= \sum_{n=0}^{N} A_n e^{i\omega_n t} \end{aligned} \tag{A.3.17}$$

This is captured in matrix-form as:

$$\begin{bmatrix} e^{-\lambda_{1,n}L_1} & e^{\lambda_{1,n}L_1} & 0 & 0 & 0 & 0 \end{bmatrix} \cdot \begin{bmatrix} \alpha_{1,n} \\ \beta 1,n \\ \alpha_{2,n} \\ \beta 2,n \\ \alpha_{3,n} \\ \beta_{3,n} \end{bmatrix} = \begin{bmatrix} A_n \end{bmatrix} \tag{A.3.18}$$

Side channel boundary condition
For the side channel we have $\phi_2(L_2,t) = \phi_0$, using the expression (A.3.7) for ϕ_2 we get:

$$\phi_2(L_2,t) = \sum_{n=0}^{N} \frac{w_i \omega_n i}{\lambda_{i,n}} \left(\alpha_n^i e^{-\lambda_{i,n}L_2} - \beta_n^i e^{\lambda_{i,n}L_2}\right) e^{i\omega_n t} = \phi_{2,0} \tag{A.3.19}$$

If we match terms with the same frequency (and divide by the prefactor), we can capture this in matrix form too:

$$\begin{bmatrix} 0 & 0 & -e^{-\lambda_n^2 L_2} & e^{\lambda_n^2 L_2} & 0 & 0 \end{bmatrix} \cdot \begin{bmatrix} \alpha_{1,n} \\ \beta 1,n \\ \alpha_{2,n} \\ \beta 2,n \\ \alpha_{3,n} \\ \beta_{3,n} \end{bmatrix} = \begin{bmatrix} 0 \end{bmatrix} \tag{A.3.20}$$

Main channel boundary condition
For η_3 we need to have that:

$$\begin{aligned} \lim_{x\to\infty} \left|\eta_3(x,t)\right| &< \infty \\ \lim_{x\to\infty} \left| \sum_{n=0}^{N} \left(\alpha_{3,n} e^{-\lambda_{3,n}x} + \beta_{3,n} e^{\lambda_{3,n}x}\right) e^{i\omega_n t} \right| &< \infty \end{aligned} \tag{A.3.21}$$

Since we have that $\mathbb{R}\mathrm{e}\{\lambda_{3,n}\} > 0$ we must have that:

$$\beta_{3,n} = 0 \tag{A.3.22}$$

And this leads to the last condition in matrix form:

$$\begin{bmatrix} 0 & 0 & 0 & 0 & 0 & 1 \end{bmatrix} \cdot \begin{bmatrix} \alpha_{1,n} \\ \beta 1,n \\ \alpha_{2,n} \\ \beta 2,n \\ \alpha_{3,n} \\ \beta_{3,n} \end{bmatrix} = \begin{bmatrix} 0 \end{bmatrix} \tag{A.3.23}$$

A.4. Salt system derivation

We start with the salt balance.

$$\frac{\partial s}{\partial t} + \frac{\phi}{wh}\frac{\partial s}{\partial x} - \mathbb{D}\frac{\partial^2 s}{\partial x^2} = 0 \tag{A.4.1}$$

We use the following ansatz for s:

$$s(x,t) = \sum_{n=-2}^{2} s_n(x) e^{ni\omega t} \tag{A.4.2}$$

Substituting this will result in the following expression:

$$\sum_{n=-2}^{2} ni\omega s_n e^{ni\omega t} + \frac{\overline{\Phi_1} e^{-i\omega t} + \overline{\Phi_0} + \Phi_0 + \Phi_1 e^{i\omega t}}{2wh} \left(\sum_{n=-2}^{2} \frac{\partial s_n}{\partial x} e^{ni\omega t} \right) - \mathbb{D} \sum_{n=-2}^{2} \frac{\partial^2 s_n}{\partial x^2} e^{ni\omega t} = 0 \tag{A.4.3}$$

Matching terms with the same frequency lead to the following equations:
For $n = -2$:

$$-2i\omega s_{-2} + \frac{\overline{\Phi_1}}{2wh} \frac{\partial s_{-1}}{\partial x} + \frac{\overline{\Phi_0} + \Phi_0}{2wh} \frac{\partial s_{-2}}{\partial x} - \mathbb{D} \frac{\partial^2 s_{-2}}{\partial x^2} = 0 \tag{A.4.4}$$

For $-1 \leq n \leq 1$:

$$ni\omega s_n + \frac{\overline{\Phi_1}}{2wh} \frac{\partial s_{n+1}}{\partial x} + \frac{\overline{\Phi_0} + \Phi_0}{2wh} \frac{\partial s_n}{\partial x} + \frac{\Phi_1}{2wh} \frac{\partial s_{n-1}}{\partial x} - \mathbb{D} \frac{\partial^2 s_n}{\partial x^2} = 0 \tag{A.4.5}$$

Lastly we have for $n = 2$:

$$2i\omega s_2 + \frac{\overline{\Phi_0} + \Phi_0}{2wh} \frac{\partial s_2}{\partial x} + \frac{\Phi_1}{2wh} \frac{\partial s_1}{\partial x} - \mathbb{D} \frac{\partial^2 s_2}{\partial x^2} = 0 \tag{A.4.6}$$

And this will results in the matrices $\mathbf{A}$, $\mathbf{B}(x)$ and $\mathbf{C}$ as defined in section 2.3.1. The next step is to create a numerical model. We use the following approximations:

$$\frac{\partial \vec{s}}{\partial x} \approx \frac{\vec{s}(x + \Delta x) - \vec{s}(x)}{\Delta x}, \quad \frac{\partial^2 \vec{s}}{\partial x^2} \approx \frac{\vec{s}(x + \Delta x) - 2\vec{s}(x) + \vec{s}(x - \Delta x)}{\Delta x^2} \tag{A.4.7}$$

And this will lead to the following matrix equation.

$$\frac{\mathbf{C}}{\Delta x^2} \vec{s}(x - \Delta x) + \left(\mathbf{A} - \frac{\mathbf{B}(x)}{\Delta x} - \frac{2\mathbf{C}}{\Delta x^2} \right) \vec{s}(x) + \left(\frac{\mathbf{B}(x)}{\Delta x} + \frac{\mathbf{C}}{\Delta x^2} \right) \vec{s}(x + \Delta x) = 0 \tag{A.4.8}$$

This can again be written in matrix form (a block matrix). We write:

$$\begin{bmatrix} \vdots & \ddots & \ddots & & \ddots & & \vdots \\ 0 & \cdots & \frac{\mathbf{C}}{\Delta x^2} & \mathbf{A} - \frac{\mathbf{B}(x)}{\Delta x} - \frac{2\mathbf{C}}{\Delta x^2} & \frac{\mathbf{B}(x)}{\Delta x} + \frac{\mathbf{C}}{\Delta x^2} & \cdots & 0 \\ \vdots & & \ddots & \ddots & & \ddots & \vdots \end{bmatrix} \begin{bmatrix} \vdots \\ \vec{s_{i-1}} \\ \vec{s_i} \\ \vec{s_{i+1}} \\ \vdots \end{bmatrix} = \begin{bmatrix} \vdots \\ \vec{0} \\ \vdots \end{bmatrix} \tag{A.4.9}$$

Bibliography

[1] Niels C. Alebregtse, H.E. De Swart, and H.M. Schuttelaars. Resonance characteristics of tides in branching channels. *Journal of Fluid Mechanics*, 728:R31–R311, 2013. doi: 10.1017/jfm.2013.319. URL https://www.scopus.com/inward/record.uri?eid=2-s2.0-84886266081&doi=10.1017%2fjfm.2013.319&partnerID=40&md5=3807387bff17c6e4eedf9d20a18c4dd4. Cited by: 14; All Open Access, Green Open Access.

[2] Carl T. Friedrichs. *Barotropic tides in channelized estuaries*, page 27–61. Cambridge University Press, 2010. ISBN 9781139487696. URL https://tudelft.on.worldcat.org/oclc/432978357.

[3] Richard Haberman. *Applied partial differential equations with fourier series and boundary value problems*. Pearson, Harlow, 5th edition, pearson new international edition edition, 2014. ISBN 9781292039855; 129203985X; 9781292053394; 1292053399. URL http://www.dawsonera.com/abstract/9781292053394.

[4] Arthur T Ippen. *Estuary and coastline hydrodynamics*. Engineering Series. McGraw-Hill Book Company, 1966. ISBN 9780070320154. URL https://tudelft.on.worldcat.org/oclc/6582037.

[5] Martijn Jorritsma. Verzilting: een bedreiging voor ons drinkwater?, September 2022. URL https://www.drinkwaterplatform.nl/verzilting-drinkwater/.

[6] Parker MacCready. Toward a unified theory of tidally-averaged estuarine salinity structure. *Estuaries*, 27(4), Aug 2004. ISSN 0160-8347. doi: 10.1007/BF02907644. URL https://doi.org/10.1007/BF02907644.

[7] Donald Samuel McLusky. *The estuarine ecosystem*. Tertiary level biology. Blackie ; Chapman and Hall, Glasgow, New York, 2nd ed edition, 1989. ISBN 0216926718; 9780216926714; 0216926726; 9780216926721; 0412020912; 9780412020919; 0412021013; 9780412021015; 0751401641; 9780751401646.

[8] Stephen G. Monismith. *Mixing in estuaries*, page 145–185. Cambridge University Press, 2010.

[9] United Nations, Department of Economic, and Social Affairs. Develop and implement a global campaign on salinization | department of economic and social affairs, May 2023. URL https://sdgs.un.org/partnerships/develop-and-implement-global-campaign-salinization.

[10] Bruce B. Parker. *Tidal Hydrodynamics*. Wiley, 1991. ISBN 9780471514985. URL https://tudelft.on.worldcat.org/oclc/23766414.

[11] Rijkswaterstaat. Zo voorkomt rijkswaterstaat dat de grootste zeesluis ter wereld het noordzeekanaal verzilt, January 2023. URL https://werkenbij.rijkswaterstaat.nl/maak-kennis/zo-voorkomt-rijkswaterstaat-dat-de-grootste-zeesluis-ter-wereld-het-noordzeekanaal-verzilt.

[12] JB Schijf and JC Schönfled. Theoretical considerations on the motion of salt and fresh water. In *Proceedings Minnesota International Hydraulic Convention*. IAHR, 1953.

[13] R. Siles-Ajamil, M. Díez-Minguito, and M.Á. Losada. Tide propagation and salinity distribution response to changes in water depth and channel network in the guadalquivir river estuary: An exploratory model approach. *Ocean & Coastal Management*, 174:92–107, 2019. ISSN 0964-5691. doi: https://doi.org/10.1016/j.ocecoaman.2019.03.015. URL https://www.sciencedirect.com/science/article/pii/S0964569118305313.